Method for Classification of Images in the Medical Field: The Nose Case

Mehdi Louizi and Mohamed Mohsen Gammoudi

***Abstract*—The tools of decision support are generally very helpful in the medical field. Indeed, it provides practitioners with complementary relevant information that may confirm their work or avoid them the use of complex search operations. It is in this context that our research work allows us in the field of ENT to automatically determine whether a nose is broken or not. We will detail throughout this article the different stages of our work which led to fracture detection results that are accurate enough according to experts.**

***Index Terms*—Component, classification of medical images, hausdorff dimension, ent, edge detection**

I. Introduction

The tools of decision support have become increasingly used by physicians because of the characteristics of medical information [1] (high dimensionality, uncertainty, vagueness, ambiguity, misinterpretation).

First, we studied the existing medical decision systems [2] -[4]. This study led us to the systems known as CBIR (Content Based Image Retrieval) [5]-[9]. Most of these systems used global descriptors to determine the overall context of the image, and then their treatment was refined by involving local descriptors. In the case of Computed Tomography images (CT) which is the context of our work, global descriptors, including the form descriptor, are essential to our method for detecting fractures, like in [10], [11]. Indeed, in this case, a single numerical value or a small set of numbers (which are then combined in a single feature vector) is used to represent the entire image [12]. We shall see later how it is implemented, with the Hausdorff dimension. We also used the geometric information of the image as a local descriptor in order to locate an area of interest from the radio image.

In our work, we focused in the field of Ear, Nose and Throat (ENT). It is a medicine branch of the medical and surgery treatment of the nose, the throat, the ear, and also the head and the neck. Practitioners are called otolaryngologists. This choice is justified by the wealth of ENT radios images and the low number of scientific work concerning the nose fractures.

In the ENT field, diagnostics may differ from whether a nose, especially the nasal bone, is fractured or not. These fractures may be not distinguishable when they are similar to bone connections or they are so small that they may not be noticed by the practitioner.

It was so necessary to propose a system able to effectively detect the presence of fractures on the nasal bone. Due to the special nature of medical images especially the DICOM format, automating the entire process from standardizing the images and detecting the nasal bone to verifying whether a fracture exists or not, requires the implementation of algorithms which are quite complex and based on physicians knowledge. Several approaches have been proposed [13] – [19] but none, in our knowledge, has treated the case of ENT. The different algorithms are, as we will mention, very specific to areas where they were employed.

For example, in the case of wrist fractures [15], used input images are MRI radio images, and detection of fracture involved the use of scintigraphy in addition to a comparison between several radios. This comparison is over the time to detect if there any evolutions or differences. The final step consists on the superposition of all these images to provide the results to several experts. Another example that we can notice is the detection of the femur and radius fractures [17], also based on the MRI radio images. Its operating principle consists on calculating the angles of the bones and using texture descriptors to identify possible fractures. Other related works are based on wavelets [19] or on multiscale methods [13], the technology of nuclear magnetic resonance [16] and ultrasonography [18]...

In this paper, we present a method for automatic detection of the nasal bone fractures. This method can be generalized in several other areas.

II. Principle of our Method

We took CT DICOM radio images as input and more specifically the sagittal section of these images. We applied our method on two different types of noses, a fractured nose, denoted by 1, and a healthy nose, denoted by 2. Our work involves three steps: (a) Isolate the nasal bone from the radio image, (b) calculate the perimeter of the nose to check if there are no fractures or discontinuities and (c) classify the different noses depending on their state.

We started by standardizing the input image in order to perform the processing operations. Indeed, the DICOM images of different patients in our possession were quite specific and it was not possible to treat them by Matlab. This is due to the specific technical characteristics of the used scanner that make certain fields (such as gray level intensity or pixel values) not readable via the usual functions of Matlab.

Then, we calculated the overall threshold of the image in order to minimize the variance between the white pixels (the bones) and the black ones. This allowed us to convert the image into a binary one.

Manuscript received May, 15, 2012; revised June 15, 2012.

Mehdi Louizi is now working as an assistant at ISSAT, Sousse, Tunisia (e-mail: mehdi@louzi.com)

Fig. 1. Standardized DICOM images

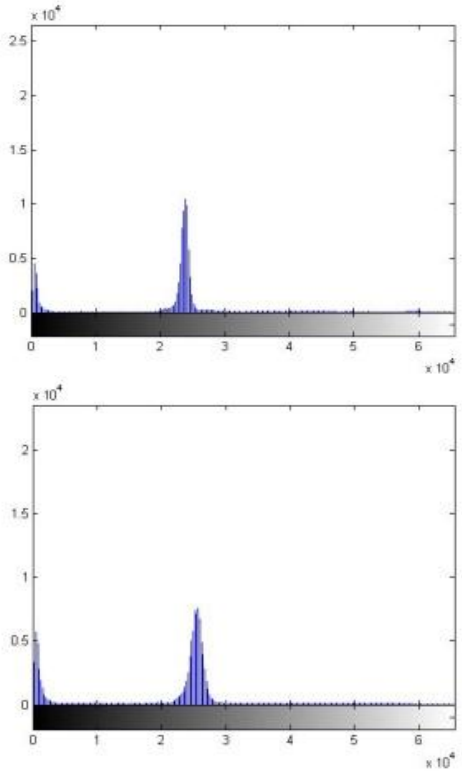

Fig. 2. Computing the overall threshold of the image

The next step is to separate the different pixels of the image; if a pixel is white we assign it the value 1 otherwise we set its value to 0. After that, successive operations of erosion and dilation (depending on the image) were applied. This has resulted in a better delineation of the different bones.

Fig. 3. Separation of image pixels

Then, we applied the Canny edge detector [20], which is one of the best algorithms in this context [21], to the grey level image in order to obtain a binary-edge map. This algorithm has been implemented on the basis of [22].

Fig. 4. Binary edge-map

Then, we extracted the edge contours from the edge-map and filled the gaps in the contours. The next step is to calculate curvature at a low scale for each contour to retain true corners.

It should be mentioned that all of the curvature local maxima are considered as corner candidates, then rounded corners and false corners (due to boundary noise and details) were eliminated.

The final step of this stage consists of adding the end points of the line mode curve as corners if they are not close to the above detected corners.

Fig. 5. Detected contours

Based on the skills of ENT experts, we calculate the lowest corner point which corresponds to the end of the nasal bone.

Fig. 6. Calculating the lowest corner point

From the previously found lowest point we implemented the algorithm “region growing” which has been applied to many similar cases [23], in order to be able to delineate the nasal bone.

The region is iteratively grown by comparing all unallocated neighboring pixels to the region. The difference between a pixel's intensity value and the region's mean is used as a measure of similarity. The pixel with the smallest difference measured this way is allocated to the respective region. [24]

This operation stops when the intensity difference between the mean region and the new pixel become larger than a certain threshold that we defined experimentally.

Fig. 7. Isolated nasal bones

At this stage, we were able to detect the nasal bone. We had to make many adjustments and corrections to have the best corresponding contours of the original images. Therefore we rebuilt our experiments several times in order to generalize this process to all samples in our possession.

After this step, we had different solutions (comparison

with an atlas of images, phase correlation ...) to answer the question "How to tell if the nasal bone is fractured or not? The first one, comparing these bones with an atlas image, as in [24] couldn't lead to good results. Indeed, given the varied characteristics of the human nose, it was not possible according to experts to define a general shape of the nasal bone. The phase correlation principle [25] could not be applied too as it is very difficult to have bones of similar or same size in order to deduce the state of a bone (fractured or not) from the other.

Thus came the idea of using the Hausdorff dimension [26] as an interesting compromise in detecting fractures of the nasal bones. Indeed, the dimension of Hausdorff offers several means of calculating the size of a metric space and has been used with encouraging results [27], in many areas. Its definition requires the study of Hausdorff H^s measures, whose formal definition is:

$$H_\delta^s(E) = \inf_{\operatorname{diam}(A_i)<\delta} \left\{ \sum_{i=1}^{\infty} \operatorname{diam}(A_i)^s : E \subseteq \bigcup_{i=1}^{\infty} A_i \right\}$$

$$H^s(E) = \lim_{\delta \to 0} H_\delta^s(E)$$

$$\dim_H(E) = \inf\{s, H^s(E) = 0\} = \sup\{s, H^s(E) = \infty\}$$

A quantitative analysis of the roughness of the perimeter is conducted to illustrate the degree of roughness of the input images. Commonly called the Hausdorff dimension (HD), the algorithm shown in Fig. 8, using the method "boxcounting [28] which generalizes the idea of counting the number of squares that cover the perimeter; the number of squares is being reduced iteratively to obtain an optimal one that gives the roughness of the whole area as a fractal dimension.

The fractal dimension describes the complexity of an object, and in our case, this algorithm gives the roughness of the perimeter that will define whether a nose is fractured or not.

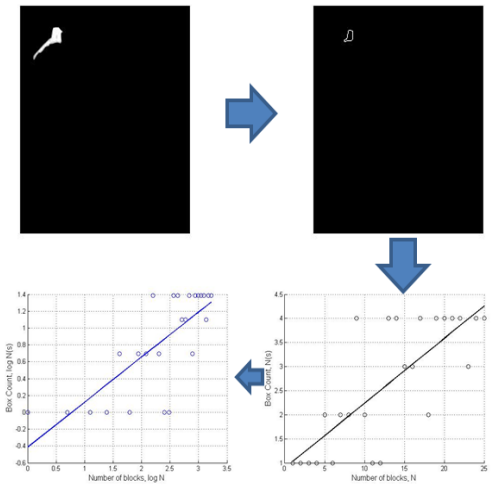

Fig. 8. Computing algorithm of the Hausdorff dimension

Thus, we obtain the Hausdorff dimension of each treated nose as a float, usually located between 0 and 1. This number will allow us to distinguish with high accuracy if the nasal bone is fractured or not.

III. Results

Our experiments were conducted on a 50 patient corpus of the hospital of La Rabta in Tunis. We have for each patient a radio image (CT) in sagittal section. The experts, the head of ENT department, the chief radio and a doctor specialized in ENT have provided us with 32 images of fractured nasal bones and 18 images of healthy nasal bone.

The tables below summarize the different results obtained.

TABLE I: Results (1)

Radio image					
fracture yes/no	yes	yes	yes	yes	yes
HD*	0,6604	0,6145	0,7281	0,6708	0,6121

*Hausdorff dimension

TABLE II: Results (2)

Radio image			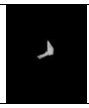	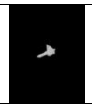	
fracture yes/no	yes	yes	yes	yes	yes
HD*	0,6772	0,9001	0, 8163	0, 7770	0, 9057

TABLE III: Results (3)

Radio image	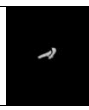			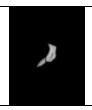	
racture yes/no	yes	yes	yes	yes	yes
HD	0, 7368	0, 7088	0, 8819	0, 9498	0, 8765

TABLE IV: Results (4)

Radio image					
fracture yes/no	yes	yes	yes	yes	yes
HD	0, 8348	0, 9921	0, 8222	0, 8190	0, 6932

TABLE V: Results (5)

Radio image					
fracture yes/no	yes	yes	yes	yes	yes
HD	0, 8851	0, 8289	0, 7305	0, 7167	0, 8301

TABLE VI: Results (6)

Radio image	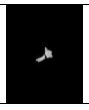	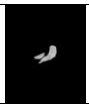			
fracture yes/no	yes	yes	yes	yes	yes
HD	0, 7883	0, 9461	0, 9362	0, 9905	0, 8285

TABLE VII: RESULTS (7)

Radio image			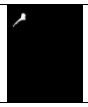		
fracture yes/no	yes	yes	yes	yes	no
HD	0, 8077	0, 9591	0, 5337	0, 5381	0, 2314

TABLE IX: RESULTS (8)

Radio image					
fracture yes/no	no	no	no	no	no
HD	0, 3656	0, 4217	0, 5247	0, 4317	0, 5245

TABLE X: RESULTS (9)

Radio image					
fracture yes/no	no	no	no	no	no
HD*	0, 5974	0, 5679	0, 5731	0, 5521	0, 5747

TABLE XI: RESULTS (10)

Radio image			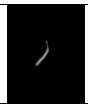		
fracture yes/no	no	no	no	no	no
HD	0, 5241	0, 5987	0, 5945	0, 3939	0, 6504

In order to automate the detection of the fracture process, it was necessary to calculate a threshold from which we can say that the nasal bone is fractured or not. This led us to search for the optimal threshold by performing several tests: accuracy versus the threshold, shown on the curve below.

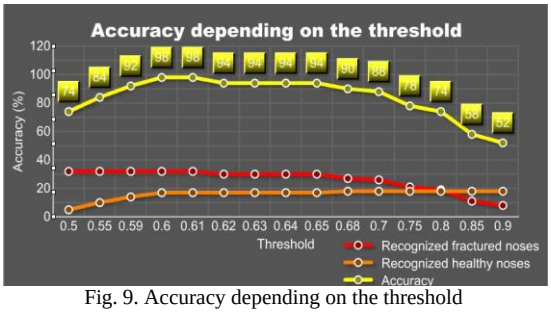

Fig. 9. Accuracy depending on the threshold

After a series of tests (15) consisting of changing the threshold each time, it was clear that the percentage of recognition of the type of nose (broken or healthy nasal bone) was highest for a threshold of 0.6. In other words, it is possible to say with an accuracy of 98%, that the Hausdorff dimension past a threshold of 0.6, clearly indicates that the nose is fractured. Below this threshold, the nose is considered healthy and not fractured.

IV. DISCUSSION / CONCLUSION AND PERSPECTIVES

Out of 50 samples that were provided to us by the hospital of La Rabta, we can conclude that only one case was detected as fractured while it was healthy. We believe that the accuracy of detection of 98% is an encouraging result for doctors but should be improved by:

- Searching for the reasons why the sample in question has not been detected as healthy.
- Extending the tests to a larger scale of radio images in order to verify the validity of our results.

We were interested in this work by a typically Tunisian test corpus. We believe in improving our experiments by obtaining radio images of foreign patients to validate our results.

REFERENCES

[1] N. Ayache, "L'analyse automatique des images médicales : Etat de l'art et perspectives," *Rapport de Recherche n°3364 - Thème 3*, INRIA - 1998.

[2] M. H. Rovner, "International collaboration in shared decision-making," The International *Shared Decision Making (ISDM) conference history and prospects*, Patient Educ Couns, pp. 01-28, 2008.

[3] M. J. Liberatore, "The analytic hierarchy process in medical and health care decision making: A literature review," *European Journal of Operational Research 189* , pp. 194–207, 2008

[4] P. Naredi, "Databases of hepatic resection for metastatic colorectal cancer—useful aids for clinical decision-making," *Surgical Oncology 17*, pp. 15–16, 2008

[5] E. Z. Barhoumi, "An Accelerated System for Melanoma Diagnosis Based on Subset Feature Selection," *Journal of Computing and Information Technology - CIT 13*, pp. 69–82, 2005.

[6] R. A. Brown, "Design of a Digital Forensics Image Mining System," *The Workshop on Intelligent Information Hiding and Multimedia Signal Processign*, 2005

[7] H. Yap, "Detecting femur fractures by texture analysis of trabeculae," in *Proc. Int. Conf. on Pattern Recognition*, 2004

[8] K. S. Fenella and P. Welsh, "Quantification of risk of a positive (R1) resection margin following hepatic resection for metastatic colorectal cancer: An aid to clinical decision-making," *Surgical Oncology 17*, pp 3–13, 2008

[9] O. A. Omiecinski, "Image Mining: A New Approach for Data Mining," *CC Technical Report GIT-CC*, 1998

[10] G. Shapiro, "Knowledge-based organ identification from CT images," (E. S. Ltd, Éd.) *Pattern Recognition*, vol. 28, no. 4, pp 475-491, 1995.

[11] S. Chaouir, "Les polyposes naso-sinusiennes - Apport de la tomodensitométrie - A propos de 41 cas," *Medecine du Maghreb n°85*, 2001

[12] B. Gouet and L. Brunet, "Connexions entre descripteurs locaux et globaux pour la reconnaissance d'objets dans les vidéos," *COmpression et REprésentation des Signaux Audiovisuels (CORESA)*, 2006

[13] D. Bereziat, "Traitement des images médicales : Détection, estimation et anaylyse du mouvement," *LIP6 - UPMC*, 2009

[14] D. Chrysostomos and V. C. Stylios, "Fuzzy cognitive map architectures for medical decision support systems," *Applied Soft Computing 8*, pp. 1243–1251, 2008

[15] D. Lepage, "Apport de la radioscintigraphie quantitative dans les traumatismes du poignet à radiographies initiales normales. Etude prospective de 154 cas," *Chir Orthop*, vol. 90, pp. 543 - 9, 2004.

[16] F. Peyrin, "Recalage d'images multimodales," *Le cahier des techniques de l'INRA - Numéro Spécial*, pp. 115-126, 2009.

[17] T. P. Tian, "Computing neck-shaft angle of femur for x-ray fracture detection," in *Proc. Int. Conf. on Computer Analysis of Images and Patterns (LNCS 2756)*, pp. 82–89, 2003.

[18] T. Petrovic, "L'échographie en médecine préhospitalière," *Urgences, Chapitre 27*, pp. 223 - 231, 2007.

[19] W. Ayadi and S. S. G. B, "Quantification des connectivités de la micro-architecture osseuse via une décomposition en paquets d'ondelettes M-bandes," *Colloque GRETSI*, 2007.

[20] J. Canny, "A computational approach to edge detection," *IEEE Trans pattern analysis*, vol. 8, no. 6, pp. 679-698, 1986.

[21] T. S. Lee, "Canny Edge Detector," *Computer Vision*, 2002

[22] X. C. He, "Corner detector based on global and local curvature properties," *Optical Engineering*, vol. 47, no. 5, 2008.

[23] N. A. M. Isa, "Seeded Region Growing Features Extraction Algorithm; Its Potential Use in Improving Screening for Cervical

Cancer," *International Journal of The Computer, the Internet and Management*, vol. 13, no. 1, pp 61-70, 2005.
[24] R. Sims, "A Pre-Clinical Assessment of an Atlas-Based Automatic Segmentation Tool for the Head and Neck," *Radiotherapy Oncology*, vol. 93, no. 3, pp. 474-478, 2009.
[25] M. Gindre, "J. Phys. IV France," Numéro C5. *3rd French* conference *on acoustics*, C5-1247 - C5-1250, vol. 4, Mai 1994.
[26] H. K. Schreiber, "Nonlinear Time Series Analysis," *Cambridge* University *Press*, 1997
[27] O. B. Zinsmeiste, "Quelques résultats sur la dimension de Hausdorff des ensembles de Julia des polynômes quadratiques," *Fundamenta* Mathematicae *151*, 1996.
[28] C. Morency, "Fractal geometry for the characterisation of urban-related states: Greater Montreal Case," *Harmonic and Fractal Image Analysis (*HARFA*)*, pp. 30 - 34, 2003

Mehdi Louizi born on August 23rd 1981 in Tunis, Tunisia, is a PHD Student at Faculté des Sciences de Tunis, Tunisia. He got his engineering degree in software engineering at INSAT, Tunisia, in 2006. Mehdi is now working as an assistant at ISSAT, Sousse, Tunisia.